OPLS5: Addition of Polarizability and Improved Treatment of Metals

Wolfgang Damm[1], Steven Dajnowicz[1], Delaram Ghoreishi[1], Yalun Yu[1], Karthik Ganeshan[1], Owen Madin[1], Benjamin Rudshteyn[1], Rui Hu[1], Meng Wu[1], Yi Shang[1], Steven Albanese[1], Yefen Zou[1], Min Ye[1], Zachary Lee Johnson[1], Michael Trzoss [1], Salma Rafi[1], Kanishk Kapilashrami[1], Noureldin Saleh[1], Phani Ghanakota[1], Yan Zhang[1], Jared M. Sampson[1], Wei Chen[1], Lingle Wang[1], Markus K. Dahlgren[1], Ellery Russell[1], Abba E. Leffler[1], Robert Abel[1], Richard A. Friesner[2], Edward D. Harder[1]*

[1] Schrödinger New York, 1540 Broadway, 24th Floor, New York, New York 10036, United States, [2]Department of Chemistry, Columbia University, 3000 Broadway, New York, New York 10027, United States,

ABSTRACT

We report on the development and validation of the OPLS5 force field. OPLS5 further extends the accuracy of our previous model (OPLS4) with the addition of explicit polarization to improve model accuracy for molecular ions and cation-pi interactions. OPLS5 also includes advances to the functional form for metals achieving significant improvements across benchmarks assessing

the structure and energetics of metal-organic complexes. Together these advances lead to improved accuracy on our protein-ligand binding benchmarks.

I. Introduction

The last decade has seen remarkable improvements in accuracy in classical force fields largely motivated by the advent of molecular mechanics based free energy methods as a critical tool in structure based drug design programs.[1] A key step in this progression was a massive scale-up in the parameterization effort needed to extensively cover drug-like chemical space at a high level of accuracy.[2] Subsequent improvements addressed chemotype transferability challenges presented by heterocyclic systems,[3] improved the balance of interactions for charged moieties[4, 5] and advanced the physics of the model to better represent anisotropic interaction features including halogen, chalcogen and lone pair hydrogen bonds.[2-4] The cumulative impact of these improvements is an accuracy level in predictions of protein-ligand binding that is now approaching the accuracy limit of the experimental data itself.[6]

To continue to make progress, further advances will require taking on some of the most challenging types of molecular interactions found in biological and materials systems. This includes systems where molecular polarizability plays an important role and thus the concomitant interactions are not well represented on average using a fixed charge force field. Here we identify and address two such regimes that arise in protein-ligand binding: (1) cation-pi interactions and (2) charged group hydrogen bonding. Likewise, owing to their more complex electronic structure and high charge concentration, interactions involving transition metals remains an area where common classical force fields tend to have high associated errors.[7, 8] Here we report on the integration of additional terms to the force field functional form to dynamically

capture metal-ligand charge transfer effects and improve the accuracy of metal-ligand interactions. Both the addition of polarizability and new metals features are encompassed in a new model termed OPLS5.

The paper is organized as follows. In section 2, we discuss the OPLS5 development. Section 2A discusses the changes made to the force field functional form. The addition of explicit polarizability to pi systems and charged moieties is discussed in 2B and 2C, respectively. The addition of charge transfer effects and the ligand field molecular mechanics model (LFMM)[9-11] to metal centers is discussed in sections 2D and 2E, respectively. In section 3 we discuss protein-ligand binding validation and section 4 summarizes the results and discusses future directions.

II. OPLS5 Developments

A. OPLS5 Functional Form

The OPLS5 functional form is given by:

Eq 1. $\mathrm{E} = E_{OPLS} + \sum_{drudes} K_D(\mathrm{r} - r_{eq})^2 + \sum_{metal\ complexes}[E_{FLucCT} + E_{AOM} + E_{Morse}]$

E_{OPLS} covers terms previously discussed,[2] including the bond stretch, angle bending, dihedral and van der Waals terms. It also includes the Coulomb potential but with changes to the available charge sites and their variability as noted below.

Intramolecular polarizability is incorporated into the model for select functional groups via the addition of classical Drude oscillators.[12, 13] These sites consist of point charge dipoles connected by a harmonic spring. The positive end is coincident with an associated heavy atom and the negative end is mobile. The Coulomb energy includes these additional charge sites with

intramolecular exclusions governed by their associated parent atom. The additional harmonic Drude self-energy term is shown in Equation 1. For any given nuclear configuration of the system the mobile Drude particles are relaxed to their energy minimum. The polarizability of each Drude oscillator can be expressed as, $\alpha_D = q_D^2/K_D$.[13] Following previous work,[12, 14] a single value Drude oscillator spring constant equal to 1000 kcal/mol/Å^2 was used for all sites. The fitting of the remaining variable, the Drude charge magnitude, is discussed in the following sections.

The remaining new terms in Equation 1 were added to describe the physics of metal complexes more accurately. This includes a morse term (E_{Morse}) to describe the interaction between metal ligand pairs and the angular overlap model term (E_{AOM}) which is an effective Hamiltonian model used to approximate d-orbital effects in transition metal complexes.[9-11] Both were discussed in more detail previously.[11, 15] To describe charge transfer and ligand polarization between metal and coordinating ligands, a dynamic fluctuating charge (FlucCT) model was developed.[16, 17] This fluctuating charge transfer model is most similar to the QTPIE model[18] but contains significant modifications that restrict charge transfer to only occur between metals and neighboring ligands. The total atomic charge is the sum of charge transfer variables (Δq_{ij}) computed from the FlucCT model plus the reference OPLS4 atomic charge (Eq. 2).

Eq 2. $$q_i = \sum_i \Delta q_{ij} + q_i^{ref}$$

The FlucCT energy is expressed in terms of Coulomb interactions with first and second order internal energy contributions.

Eq 3. $$E(\Delta q) = \sum_{ij} f_{ij}\left(\chi_{ij} + \phi_{ij}\right)\Delta q_{ij} = + \sum_{ij}\sum_{kl} \Delta q_{ij} J_{ij,kl} \Delta q_{kl}$$

Here, χ_{ij} is the difference in the ligand and metal electronegativities, and ϕ is the difference in the reference "fixed charge" electrostatic potential between the ligand atom and metal ion. The term J

contains self-coulomb contributions along with screened Coulomb interactions between charge transfer variables. Like in the QTPIE model[18] a screening function (f_{ij}) is used to ensure the charge transfer vanishes outside the cutoff radius. Here, we use a sigmoid function (Eq. 4) for the screened interactions.

Eq 4. $$f_{ij} = \frac{1}{1+e^{k_0(r_{ij}-r_0)}}$$

Where k_0 and r_0 are global parameters, which determine the rate and midpoint respectively. Minimizing the FlucCT energy with respect to all the charge transfer variables leads to a system of linear equations that can be solved numerically.

In the implementation of the model discussed herein we employ an additional approximation where the Drude polarizabilities are set to zero for metal containing systems employing the FlucCT and LFMM metals functionality. Additional development continues to further integrate these terms together.

B. Cation-Pi Interactions

Induced polarization of aromatic pi-systems plays a significant role in defining the strength of cation-pi interactions[19] but is completely absent in most standard fixed charge force fields.[4, 20, 21] In OPLS5 we include these effects by adding polarizable Drude oscillators to the heavy atoms of aromatic functional groups.

The Drude parameters were developed as follows. A 1.0e test charge probes the out-of-plane polarization energy for the aryl systems studied. An example coordinate for benzene is shown in Figure 1, where the probe distance extends from the ring center, perpendicular to the ring plane. Model polarizabilities are varied to match the QM interaction energy at distances

between 3.5-4.0 angstroms, commensurate with cation-pi interaction distances observed experimentally.[22] A comparison between QM and MM over a scan of candidate model polarizabilities is shown for benzene in Table 1 where an $\alpha_D = 1.0$ Å^3 agrees best with QM and is used in OPLS5. To extend the coverage to other aryl heterocycles, additional coordinates were developed covering the 5 and 6-membered aromatic ring systems shown in Figure S1. OPLS5 polarizability parameters are summarized in Table S1. An additional aryl carbon/water oxygen specific vdw parameter (Table S2) was introduced and fit against the benzene-water dimer interaction energy shown in Figure S2 and the benzene hydration free energy. To further validate the model, we tested a set of heterocyclic systems with available aqueous solvation free energies which is summarized in Table 2, showing improved accuracy with OPLS5.

C. Charged System Hydrogen Bonding

In our recent study of molecular ions[4] we noted the significant role polarization plays in modulating the strength of hydrogen-bonds to charged species subject to the species dielectric environment. Fixed charged models, like OPLS4[4], aim to capture the mean field strength of these interactions but tend to fail when the surrounding environment deviates significantly from that ideal. To improve the accuracy of the model across more diverse environments, we extend the nonbonded representation of OPLS5 with additional polarizable Drude sites for target charged species.

Polarizability parameters were taken from earlier work[23] and are summarized for the supported systems in Table S1. Subsequent refinement of associated vdw parameters followed by scanning candidate vdw radii and selecting parameters that gave the best agreement to QM interaction energies and experimental protein pK_a's. Results for ion-water interaction energies are summarized in Table 3 and show a marked improvement over OPLS4[4]. The configurations

are taken from the cluster systems studied in Figure 2 of Lu et al.[4] The optimized OPLS5 sigma parameters are shown in Table S3.

Additional pair-specific vdw parameters were then added and tuned to experimental salt-association data. Data is available for two systems of interest, acetate-guanidinium and acetate-butylammonium.[24] Experimentally, the salt-bridge strength is assessed by measuring the shift in acetate pK_a that occurs in solution with these counter cations. The stronger the salt-bridge interaction the more the charged form of acetate is stabilized leading to smaller measured pK_a*'s*. Acetate-tetramethylammonium is used as a reference to control for the influence of ionic strength on the measurements. The simulation method used to get the model values is described in section S2a. Optimized parameters are given in Table S4. Results comparing these pK_a shifts for both OPLS4 and OPLS5 are shown in Table 4. Both models are in excellent agreement with experiment though OPLS4 slightly over-estimates the salt-bridge strength.

In a last step, protein side chain torsion parameters for aspartate, glutamate and histidine were re-optimized. In the development of OPLS4[4] we observed and leveraged the sensitivity of protein pK_a predictions to the χ_1 torsion parameters of the force field to refine these parameters. We repeat that exercise here for OPLS5. Candidate models are first generated that remain consistent with statistical X-ray and neutron scattering rotamer populations (see section S2b for additional details). Then the best performing model against the pK_a benchmark assembled in reference[5] is selected. Results are summarized in Table 5 where OPLS5 shows comparable accuracy to OPLS4 for ASP and HIS and gives a 14% improvement in accuracy for GLU.

D. Metal-Ligand Charge Transfer

Fixed charge force fields, including OPLS4[4], restrict the represented charge of metal atoms to their associated oxidation state. However, QM electrostatic potential calculations indicate that, in coordination complexes, a significant amount of this charge is shared with the coordinating ligands. Two examples are shown in Figure 2 and highlight the degree to which OPLS4[4] fails to capture the charge distribution in these complexes. Most notably, according to QM, 1.5e and 0.7e of charge, respectively, is transferred to the coordinating ligands. This effect is missing in the OPLS4 model, limiting its ability to accurately represent the electrostatic properties of the complex. To accurately represent the charge distribution of these complexes in a dynamic fashion, we employ the FlucCT model described in Section 2.

Our primary focus is to construct general coverage around common chemistries found in two application regimes: (1) metalloenzyme systems and (2) Pt(II) and Ir(III)-based phosphorescent emitters used in OLED materials. The metal centers of interest are Mg(II), Ca(II), Zn(II), Fe(II), Fe(III), Pt(II) and Ir(III). An initial dataset was constructed by querying the Cambridge Structural Database (CSD)[25] for metal-organic compounds containing Platinum or Iridium. In addition, the PDBbind database[26] was used to query metalloenzymes with drug-like molecules bound near (< 5.0 Å) metal ions. Fragment representations of mono-metal complexes were extracted from the crystal structures and any counterions were removed, resulting in 1000s of complexes. The initial dataset was further refined by filtering out highly charged complexes ($|\text{total charge}| \geq 2$), rare chemistries, and duplicates. For the Ir(III) and Pt(II) subset, complexes that did not contain at least one aromatic ligand were also filtered. These series of filters resulted in our final data set, which contains ~500 unique complexes.

The geometries of the final data set were optimized using DFT at the ωB97x-D3/lacvp+*[27, 28] level of theory, in an effort to fix any poor placement of hydrogens. The target properties for

model training were computed using DFT. For FlucCT, the electrostatic potential (ESP) of the optimized geometry was computed with and without an external uniform electric field (-0.02 a.u. in either x, y, or z directions) at the ωB97x-D3/lacvp+*[27, 28] level of theory.

The sigmoid screening function was designed to taper off when charge-transfer effects become negligible. Based on a study of a small set of prototypical complexes we found values of k_0=1.5 Å^{-1} and r_0=4.5 Å worked well in this regard. The self-hardness parameters (J_{ii}) and metal and ligand electronegativities (χ_i) are delineated in the model by atom types and are fit as follows. First the FlucCT parameters were optimized by minimizing the RMSE of the ESP with and without an external uniform electric field. We found that providing radial scan interaction energy data (described in the following section) at the DFT minima and further away (~5.0 Å) improved the overall performance by providing additional information regarding the polarization response. These relative energies were included into the loss function with a small weight (0.005 compared to the ESP weight of 1.0) if the FlucCT model was more attractive compared to DFT. A summary of the respective models' ability to reproduce the QM ESP is summarized in Table 6. A dramatic improvement in accuracy (~70% improvement) is observed for OPLS5.

E. Morse and AOM Parameterization

After the FlucCT parameters are determined, the Morse and AOM model parameters are optimized against a series of rigid metal-ligand radial scans and ligand rotations. These scans are performed on the same set of fragment complexes used in FlucCT training, with relative energies computed at the ωB97x-D3/def2-tzvpd(-f)[28, 29] level of theory. Parameters are then fit to best match DFT relative energies. The training set results are summarized in Table 7.

For Pt(II) and Ir(III) complexes, we found that scaling the metal Lennard-Jones sigma parameters by a factor of 0.92x improved the metal-ligand equilibrium distances. In addition, a scale factor of 0.5 is applied to 1,4 pairs for negatively charged biaryl bidentate ligands. The final OPLS5 model has an RMSE of 0.07 Å for metal-ligand equilibrium distances, a weighted RMSE of 5.4 kcal mol^{-1} for metal-ligand radial scan relative energies, and a weighted RMSE of 3.9 kcal mol^{-1} for the ligand rotation relative energies. Again, this is a significant improvement compared to OPLS4, which has a RMSE of 0.3 Å for metal-ligand equilibrium distances, a weighted RMSE of 32.6 kcal mol^{-1} for metal-ligand radial scans relative energies, and a weighted RMSE of 8.0 kcal mol^{-1} for the ligand rotations relative energies. Here, the weights are the Boltzmann weights that are used during fitting. The final model was further validated against DFT optimized geometries from an independently curated test set containing ~500 complexes. The overall mean RMSD on the test set is 0.5 Å and 1.9 Å for OPLS5 and OPLS4 respectively. Examples showing the improved geometries with OPLS5 are shown in Figure 3.

III. Application to Protein-Protein and Protein-Ligand Binding

A. Overview.

In reference[6] we assembled the largest publicly available data set of protein-ligand binding systems suitable for benchmarking FEP methods and used it to assess the accuracy of FEP+[30] with the OPLS4[4] force field. Here our aim is to further extend this benchmark and use it to assess the performance of OPLS5.

B. Polarizability.

Given the primary purpose is to assess force field accuracy, the benchmark used in the present work includes some changes to minimize uncertainty from other factors including uncertain ligand pKa's, poor sampling etc. discussed in more detail in Section S3a. Additional series were also selected that probe chemical transformations where we suspected polarizability to play an impactful role in the binding process. These systems include 4 series exploring cation-pi interactions in the S4 pocket of FXA,[31] a recently published zwitterion series[32] and a series binding to the FGFR3 protein that modulate ligand-protein salt-bridge interactions and a protein-protein binding system that includes a series of mutations modifying the interaction environment of interfacial charged residues.[33] Three additional series with a similar chemistry focus were sourced from Schrödinger discovery projects. The FEP+ protocol used in all calculations was the same used in Lu et al.[4]

Performance of OPLS4[4] and OPLS5 is summarized in Table 7, where the reported errors are averaged over the following twelve data sets: (1) R-group modifications (2) heterocycle transformations (3) displacement of binding site waters (4) net charge changes (5) the Merck benchmark (6) fragments (7) Janssen BACE1 systems (8) MCS docking (9) scaffold hopping (10) macrocycles (11) miscellaneous and (12) polarizability cases. Results for each individual system are provided in Table S5. Relative to OPLS4, the overall RMS error is improved with OPLS5 by approximately 5%. This improvement is driven by the new systems selected to highlight challenging polarizability cases. There, OPLS5 gives a 30% improvement in accuracy. An example perturbation that highlights the improvement across the FXA cation-pi systems is shown in Figure 4, where a t-butyl group residing in the S4 pocket is replaced with a similarly sized tetra-methyl ammonium. Experimentally, this change is favored by -2.4 kcal/mol. The predicted change in potency with OPLS4 is -0.5 kcal/mol, significantly under-estimating the gain

in affinity observed experimentally. This is consistent with the model missing three key potential cation-pi interactions to Phe174, Tyr99 and Trp215. In contrast, the addition of polarizability to aryl groups in OPLS5 picks up on these interactions resulting in a more significant gain in potency (ddG = -2.4 kcal/mol) in-line with experiment. Similar perturbations are found in all 4 of the new FXA series and account for the significant across-the-board improvement for this subgroup as shown in Table S5.

Another example of the improved treatment of cation-pi interactions in OPLS5 translating to more accurate predictions is observed in the Fc-FcRn system. Specifically, as shown in Figure 5 the mutation of Met252 into tryptophan is favored experimentally[34] by -1.1 kcal/mol but disfavored by the same amount using OPLS4. OPLS5 recovers this trend correctly predicting the relative binding of the tryptophan mutant (ddG = -0.8 kcal/mol). The main driver of this change in potency is the two cation-pi interactions to Lys248 and Arg255 that form to Trp252 in the bound complex.

Across the "polarization" systems, one of the most significant improvements is seen for the FGFR3 system (see Section S4 for experimental data details). The OPLS4 RMSE=2.9 kcal/mol whereas the OPLS5 RMSE is 1.6 kcal/mol. OPLS4 significantly overpredicts the potency of a subset of ligands which all include the addition of alkyl ammonium substituents that form a salt-bridge to a neighboring aspartate. An example perturbation is shown in Figure 6. Experimentally this addition is disfavored (ddG = 3 kcal/mol). In contrast, OPLS4 predicts the addition to be favored by -0.6 kcal/mol. This large over-prediction is seen despite specific tuning of the salt-bridge strength in OPLS4 and extensive validation of this feature to salt-bridge strength sensitive experimental data.[4] What distinguishes this system from the typical salt-bridge systems represented in the previous validation studies is the nature of the electrostatic environment

surrounding the formed salt-bridge. As shown in Figure 6, the aspartate is involved in two simultaneous interactions to both the ligand on the right and a neighboring lysine. The lysine competes with the polarization response contribution to the salt-bridge strength weakening the interaction relative to that modeled by a simple fixed charge model like OPLS4. In contrast, the addition of polarizability to OPLS5 better captures this environmental modulation of the salt-bridge interaction leading to a significant improvement in the associated FEP prediction (ddG = 1.4 kcal/mol).

C. Metalloenzymes.

Owing to their chemical complexity and the purported lack of accuracy in current force fields, one class of systems that has been considered outside the current domain of applicability for methods like FEP+ are metalloenzymes. This is also reflected in the lack of representation of such systems in published benchmarks. Here we aim to assemble a suitable data set to characterize the accuracy limitations of OPLS4 and the potential improvements seen with the advanced functional form features for metal-ligand interactions included in OPLS5. The data set is subdivided into two parts based on proximity to the metal complex: (1) perturbations near the metal-organic complex and (2) perturbations that directly modifies one of the groups coordinating the metal.

The near-complex systems include ligands binding to MMP13 near the Zn^{2+} complex, a series of PDE1B inhibitors binding near the Zn^{2+}/Mg^{2+} di-metal complex and 6 additional series sourced from internal Schrödinger programs. The results are summarized in Table 8. The overall RMSE for OPLS4 is 1.9 kcal/mol well-above the accuracy threshold of approximately 1.2 kcal/mol observed for non-metal systems. In contrast OPLS5 significantly improves upon

this leading to an accuracy of 1.3 kcal/mol. The large observed OPLS4 error is a product of the erroneous approximation made by the model in its representation of the charge distribution of the complex. In particular, the model misses the nearly full electron of charge that's shared with its complexed neighbors. An example perturbation that highlights this driving force is shown in Figure 7 for the MMP-13 system. The perturbation involves changing the para-fluoro substituent to a methoxy group. The proximity of the substituent position next to the Zn^{2+} complex makes it sensitive to the force fields representation of the charge distribution. Experimentally the affinity change is nearly equipotent (ddG=-0.3 kcal/mol) whereas OPLS4 erroneously predicts a significant loss in potency for the methoxy substituent (ddG=+2.8 kcal/mol). To specifically test the impact from complex charges we also ran a model of OPLS4 that simply replaces the charges of the zinc complex with QM fit custom charges (OPLS4cc) which fixes the prediction error (ddG=+1.1 kcal/mol). The fluctuating charge model in OPLS5 effectively recapitulates the QM-like charge distribution leading to a similar prediction.

IV. Conclusion

We report on a new version of the force field, OPLS5, that improves protein-ligand binding affinity accuracy by addressing previous limitations in the representation of electronic polarization and the modeling of transition metal-organic complexes.

It is worth touching on how the accuracy improvement, from the addition of polarizability, is distributed across the protein-ligand binding data set. Notably, the improvement is concentrated amongst the test cases where polarization effects were hypothesized to play a significant role while the performance on the remaining "non-polarizable" test cases remains very similar to OPLS4. This result supports the view that the fixed charge approximation works well for

predicting binding free energies across most functional groups and structural contexts. That is despite many of these data sets (eg. the pKa data set) being quite sensitive to the electrostatic model. This result also provides validation of our parameterization strategy (i.e. targeting the addition of polarizability to only a subset of moieties) and, further, is indicative of a well-balanced model. In effect, OPLS5 capably addresses systems where the fixed charge approximation breaks down while maintaining the excellent performance seen with OPLS4, otherwise. As a contrast, it would be interesting to investigate polarizable force fields in the literature that were developed from scratch and interrogate their ability to reproduce the free energy changes for the FEP data sets covered herein.

The results reported above do leave one with the question as to the source of the remaining residual errors. One possibility is that further refinements to the present Drude model are required including extending the coverage of polarizable groups, and we intend to continue investigating this possibility in future work. However, it is also likely we are reaching the fundamental limits of the FEP testing and optimization paradigm that has worked well to drive force field improvements for the past 10 years. Noise in experiments measuring binding affinities are typically on the order of 0.5-1 kcal/mol RMS error. Some amount of noise is similarly present in the computations due to imperfect sampling. In principle these issues could be addressed systematically by increasing experimental precision, while at the same time using a more thorough conformational search algorithm for initial ligand placement, coupled with more extensive sampling in the FEP runs. We see exploring this direction as a key next step in our efforts to produce the most reliable rank ordering possible for candidate ligands in drug discovery programs.

Work on metal containing force fields is at an early stage. While the improvements outlined above appear highly promising, proving out the value of OPLS5 for these systems will require further development to improve the coverage of the model as well as application to a large number of projects, both at Schrödinger and in the hands of other users of FEP+. We expect to report on such efforts in future publications.

Figures and Tables

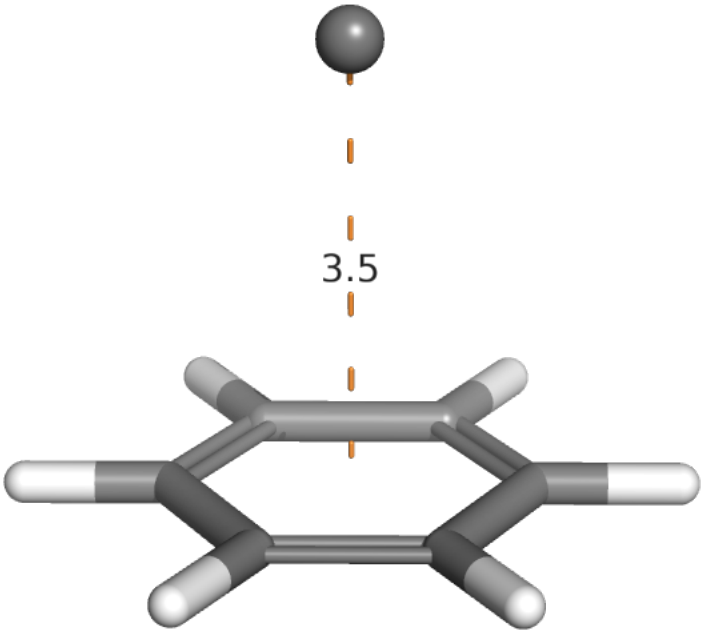

Figure 1. Probe charge position used to parameterize the polarizable Drude parameters.

Table 1. Test charge interaction energy (kcal/mol) for the benzene system shown in Figure 1.

Probe Distance	QM	α=0	α=1.0	α=1.5	α=2.0
3.5 Å	-13.6	-7.4	-12.7	-15.3	-17.8
4.0 Å	-9.5	-5.4	-8.8	-10.4	-12.0

*QM evaluated at the wB97X-D/6-311++G** level.

Table 2. Hydration free energies for small aromatic molecules impacted by the OPLS5 parameter changes (kca/mol).

Compound	Exp.	OPLS4	OPLS5
Benzene	-0.9	-1.3	-0.9
Toluene	-0.9	-0.9	-0.7
Pyridine	-4.7	-4.3	-4.5
2-methyl pyrazine	-5.5	-6.5	-6.6
3-Methylindole	-5.9	-5.2	-5.3
Pyrrole	-4.8	-5.5	-4.9
1-methyl pyrrole	-2.9	-3.9	-3.1
imidazole	-9.6	-9.0	-9.5
N-methylimidazole	-8.4	-7.4	-7.9
4-methyl-1h imidazole	-10.3	-8.7	-9.6
Thiophene	-1.4	-1.3	-1.2
2-methyl thiophene	-1.4	-1.0	-1.3
Thiazole	-4.2	-4.6	-4.7
RMS error		0.76	0.46

Table 3. Interaction energy comparison for configurations in Figure 2 of Lu et al.[4] that have changed in OPLS5 (kcal/mol)

Group	CCSD(T) /CBS	OPLS4	OPLS5
Acetate	-10.5	-11.3	-10.5
Guanidine	-10.0	-11.9	-11.2
Ethyl ammonium	-12.8	-14.1	-13.8
Ethyl-methyl ammonium	-14.3	-15.1	-14.4

Ethyl-dimethyl ammonium	-15.8	-16.6	-15.8
Ethyl-Imidazolium	-15.0	-16.0‡	-15.5
Mean Signed Error		-1.1	-0.5

‡OPLS4 value for ethyl-imidazolium changed since reference[4] due to a vdw parameter change for the imidazolium nitrogen.

Table 4. Acetate pK_a shift (in pK_a units) from a 1 *M* tetramethylammonium chloride solution to a 1 *M* guanidinium chloride or methylammonium chloride solution.

System	Exp.	OPLS4	OPLS5
Acetate-guanidinium	-0.136	-0.26	-0.14
Acetate-butylammonium	-0.118	-0.26	-0.07

Table 5. Root mean square errors in kcal/mol for the aspartic acid, glutamic acid and histidine pKa sets (kcal/mol).

Amino acid	Number	OPLS4	OPLS5
ASP	33	0.75	0.76
GLU	44	0.70	0.61
HIS	64	0.80	0.79

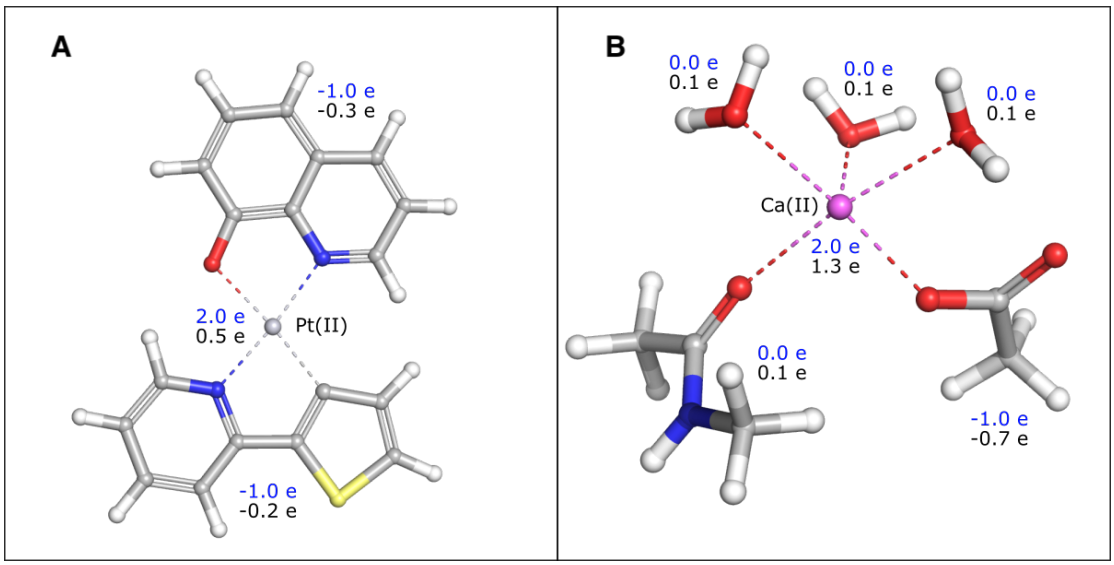

Figure 2: Examples of charge transfer. In panel A, a platinum complex taken from the Cambridge structural database (WESRES) and in panel B a representative fragment of the bound calcium complex in the PDB structure 2GVV. The total charge of each molecule and metal ion are in blue for OPLS4 and black for QM ESP-based charges.

Table 6. OPLS4 and OPLS5 model performance (RMSE) comparison of electrostatic potential relative to QM (kcal/mol/e)

	OPLS4	OPLS5
No external field	16.6	2.9
W. external field	20.6	7.3

Table 7. OPLS4 and OPLS5 model performance (weighted RMSE) comparison of relative energies (kcal/mol) compared to QM

	OPLS4	OPLS5
Ligand Rotations	7.4	3.9
Radial Scans	32.6	5.4

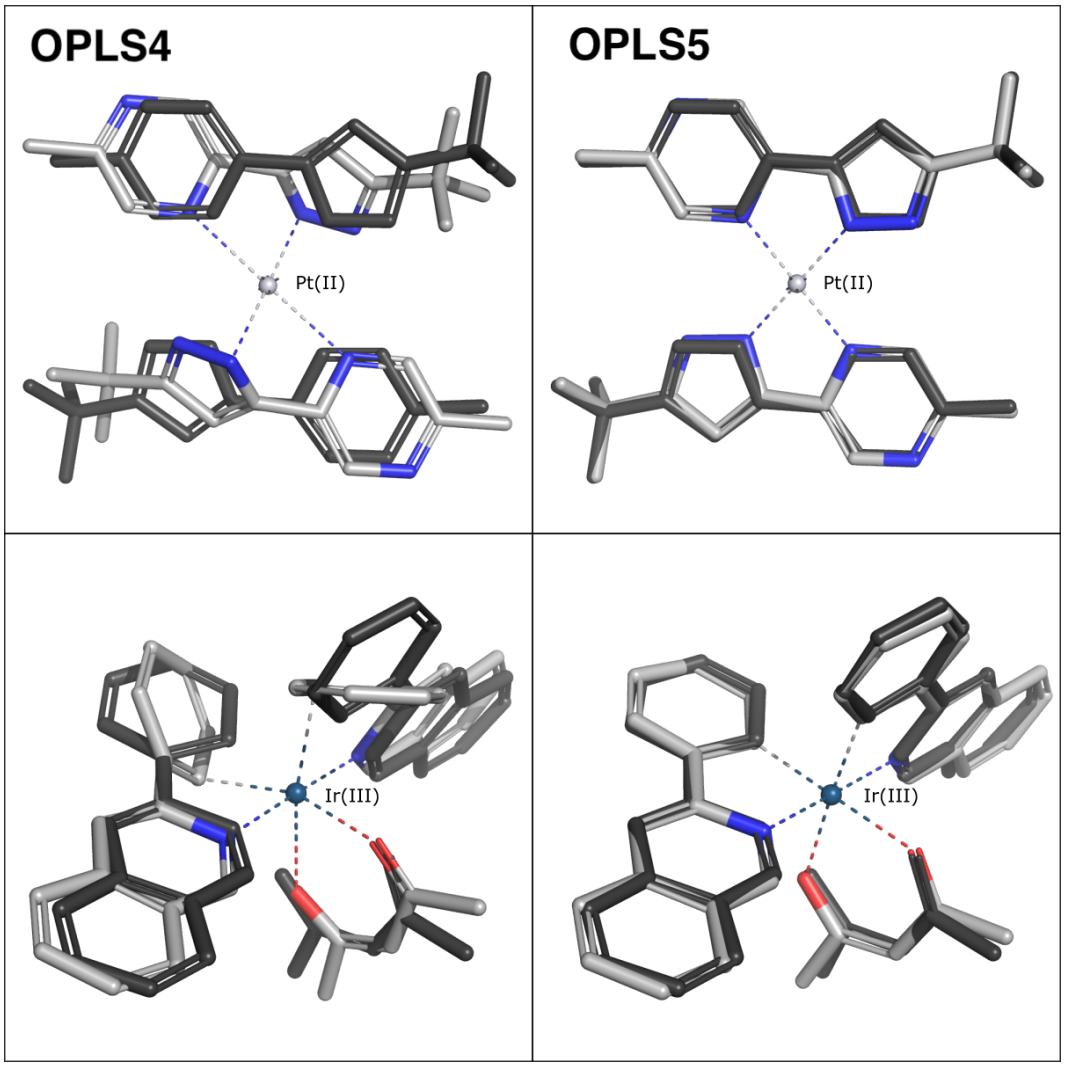

Figure 3. Examples of improved metal-complex geometries. QM and MM optimized geometries in dark and light grey, respectively.

Table 7. Root mean square errors for relative binding free energy results (kcal/mol).

Perturbation Class	No. cmpds	OPLS4		OPLS5	
		Edgewise	Pairwise	Edgewise	Pairwise
R-group	199	0.93	1.06	0.99	1.13
Heterocycle Focused	200	1.18	1.33	1.19	1.31
Water Displacement	65	1.12	1.19	1.13	1.15

Charge Change	53	1.17	1.18	1.16	1.17
Merck	238	1.18	1.37	1.17	1.38
Fragments	79	0.94	1.08	0.91	1.02
Janssen BACE1	74	1.15	1.17	1.16	1.19
MCS docking	49	1.56	1.38	1.25	1.34
Scaffold hopping	21	0.79	0.75	0.75	0.83
Macrocycles	58	1.09	1.30	1.12	1.41
Misc	79	0.96	1.02	0.92	0.96
Polarizability	68	2.0	2.1	1.38	1.48
Total Weighted Average	1183	1.18	1.29	1.12	1.25

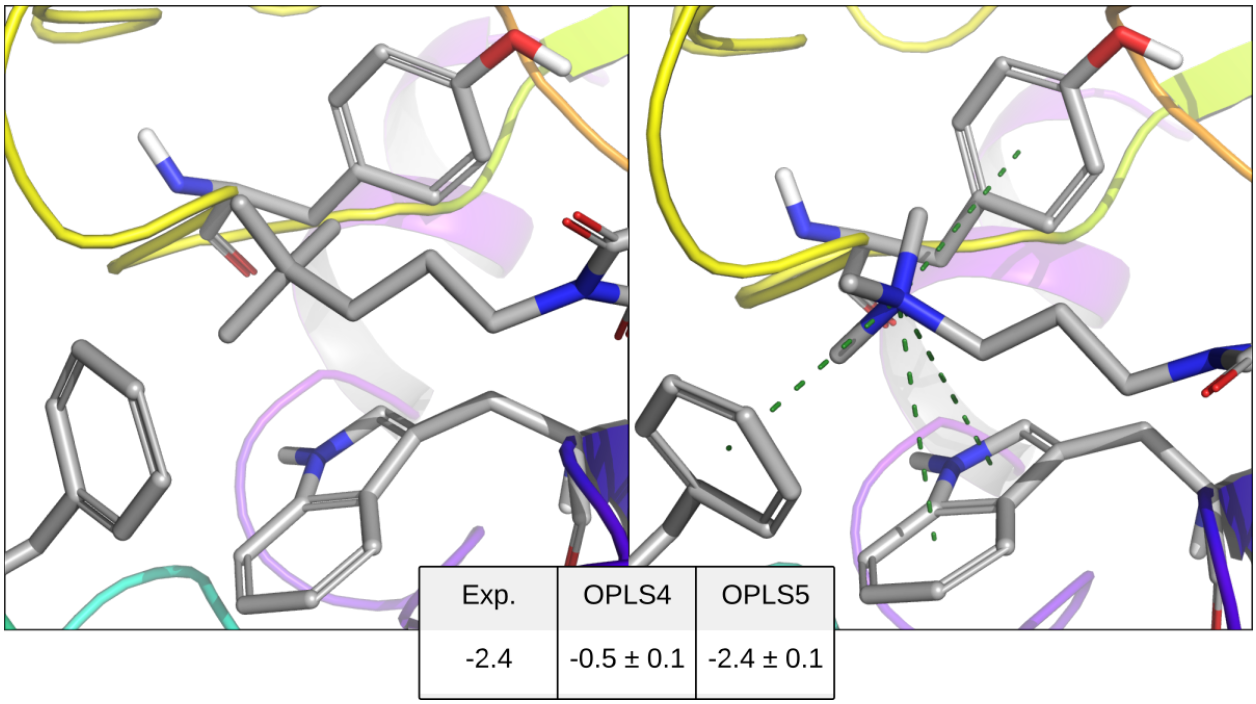

Figure 4. Experimental and FEP-predicted relative binding free energy (kcal/mol) for replacing t-butyl substituent with tetra methyl-ammonium in the S4 pocket of FXA.

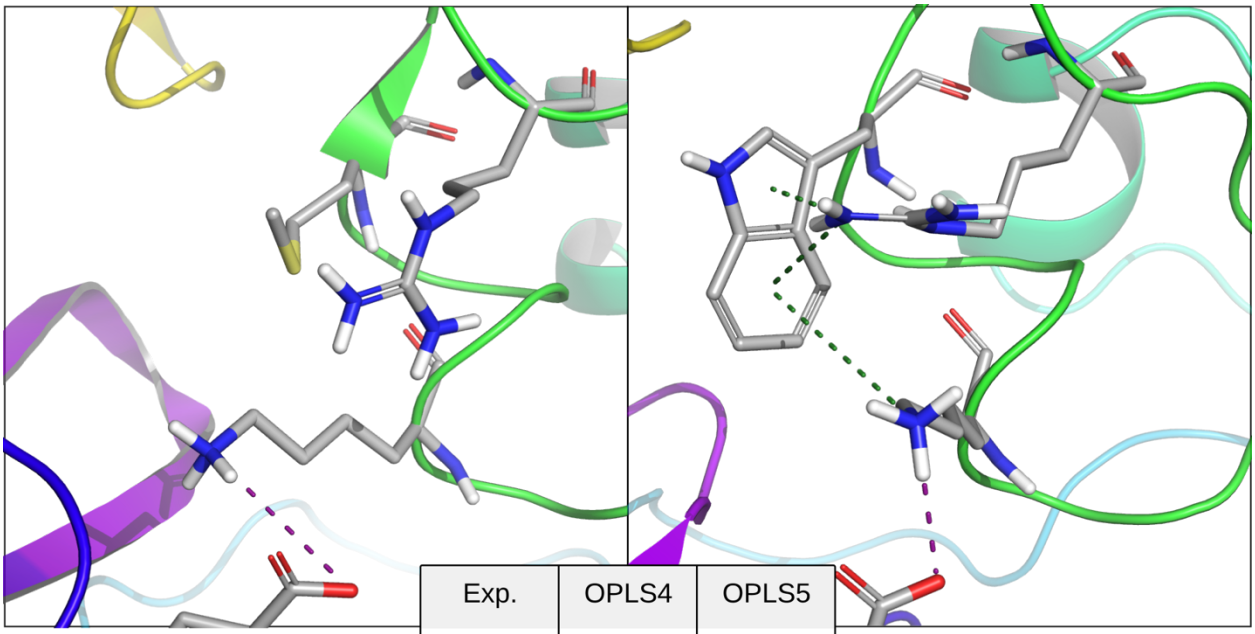

Exp.	OPLS4	OPLS5
-1.1	1.1 ± 0.2	-0.8 ± 0.3

Figure 5. Experimental and FEP-predicted relative binding free energy (kcal/mol) between wild-type Fc and a mutant (MET252TRP) to the FcRn receptor.

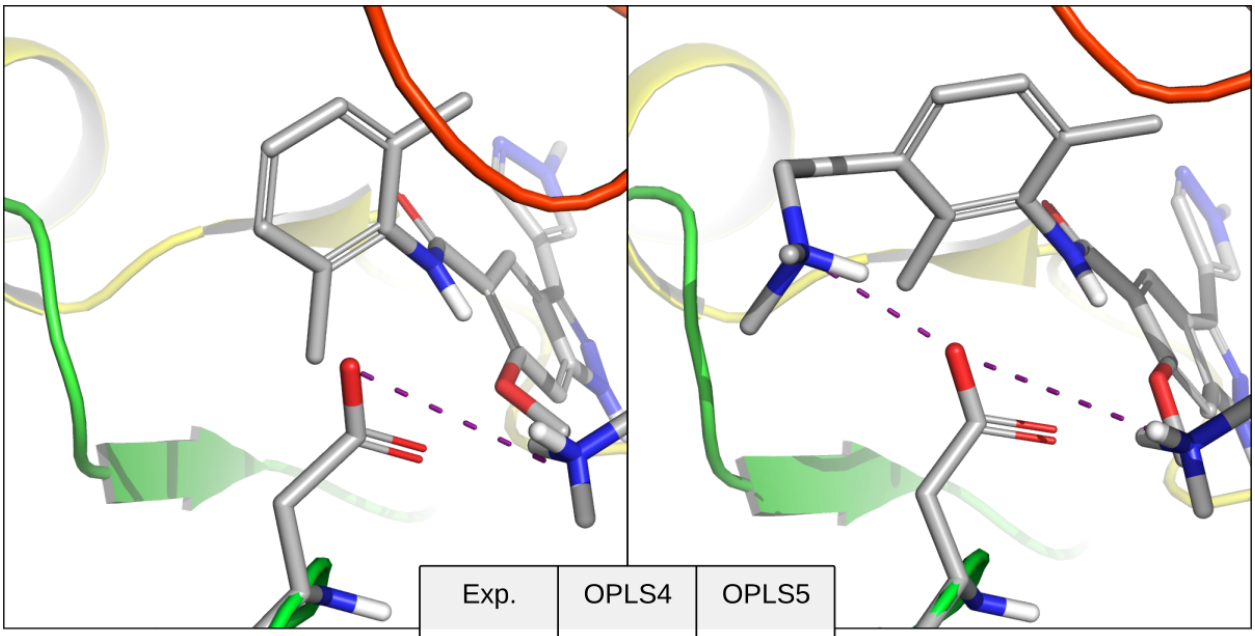

Exp.	OPLS4	OPLS5
3.1	-0.6 ± 0.2	1.4 ± 0.1

Figure 6. Experimental and FEP-predicted relative binding free energy (kcal/mol) for ethyl-ammonium addition to phenyl ring in FGFR3.

Table 8. Binding free energy results for FEP+ perturbations near bound metal-organic complexes.

System	No. cmpds	RMSE (kcal/mol)	
		OPLS4	OPLS5
PDE1B	13	1.3	1.4
MMP13	29	1.7	1.3
Project I	14	1.3	0.9
Project J	4	1.3	1.3
Project K	4	0.4	0.9
Project L	18	2.1	1.0
Project M	19	1.9	1.8
Project N	9	3.7	1.6
Total Weighted Average	110	1.9	1.3

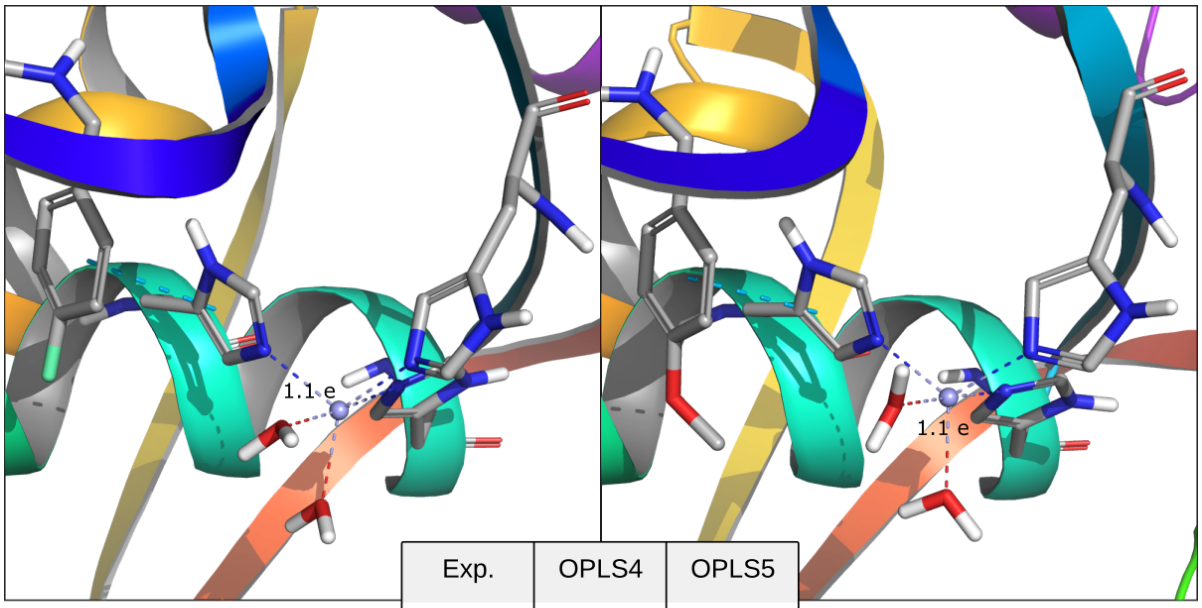

Figure 7. Experimental and FEP-predicted relative binding free energy (kcal/mol) in MMP13. Charge on metal is from a QM ESP calculation indicating ~1e of charge transfer to coordinating ligands.

AUTHOR INFORMATION

Corresponding Author

* ed.harder@schrodinger.com

Notes

Atomic coordinates and structure factors for the reported FGFR3 crystal structure have been deposited in the Protein Data Bank under accession code 9D1X. The authors declare the following competing financial interest(s): R.A.F. has a significant financial stake in, is a consultant for, and is on the Scientific Advisory Board of Schrödinger, Inc. We would like to thank Sandra Postel, Robert Byrne and Stephen Fullerton from Crelux for helping to determine the FGFR3 crystal structure.

REFERENCES

(1) Knight, J. L.; Leswing, K.; Bos, P. H.; Wang, L. Impacting drug discovery projects with large-scale enumerations, machine learning strategies, and free-energy predictions. In *Free Energy Methods in Drug Discovery: Current State and Future Directions*, ACS Publications, 2021; pp 205-226.
(2) Harder, E.; Damm, W.; Maple, J.; Wu, C.; Reboul, M.; Xiang, J. Y.; Wang, L.; Lupyan, D.; Dahlgren, M. K.; Knight, J. L.; et al. OPLS3: A Force Field Providing Broad Coverage of Drug-like Small Molecules and Proteins. *Journal of Chemical Theory and Computation* **2016**, *12* (1), 281-296. DOI: 10.1021/acs.jctc.5b00864.
(3) Roos, K.; Wu, C.; Damm, W.; Reboul, M.; Stevenson, J. M.; Lu, C.; Dahlgren, M. K.; Mondal, S.; Chen, W.; Wang, L.; et al. OPLS3e: Extending Force Field Coverage for Drug-Like Small Molecules. *Journal of Chemical Theory and Computation* **2019**, *15* (3), 1863-1874. DOI: 10.1021/acs.jctc.8b01026.
(4) Lu, C.; Wu, C.; Ghoreishi, D.; Chen, W.; Wang, L.; Damm, W.; Ross, G. A.; Dahlgren, M. K.; Russell, E.; Von Bargen, C. D.; et al. OPLS4: Improving Force Field Accuracy on Challenging Regimes of Chemical Space. *J Chem Theory Comput* **2021**, *17* (7), 4291-4300. DOI: 10.1021/acs.jctc.1c00302 From NLM PubMed-not-MEDLINE.
(5) Coskun, D.; Chen, W.; Clark, A. J.; Lu, C.; Harder, E. D.; Wang, L.; Friesner, R. A.; Miller, E. B. Reliable and Accurate Prediction of Single-Residue pKa Values through Free Energy Perturbation Calculations. *Journal of Chemical Theory and Computation* **2022**, *18* (12), 7193-7204. DOI: 10.1021/acs.jctc.2c00954.

(6) Ross, G. A.; Lu, C.; Scarabelli, G.; Albanese, S. K.; Houang, E.; Abel, R.; Harder, E. D.; Wang, L. The maximal and current accuracy of rigorous protein-ligand binding free energy calculations. *Communications Chemistry* **2023**, *6* (1), 222. DOI: 10.1038/s42004-023-01019-9.
(7) Li, P.; Merz Jr, K. M. Metal ion modeling using classical mechanics. *Chemical reviews* **2017**, *117* (3), 1564-1686.
(8) Bursch, M.; Hansen, A.; Pracht, P.; Kohn, J. T.; Grimme, S. Theoretical study on conformational energies of transition metal complexes. *Physical Chemistry Chemical Physics* **2021**, *23* (1), 287-299.
(9) Deeth, R. J. The ligand field molecular mechanics model and the stereoelectronic effects of d and s electrons. *Coordination Chemistry Reviews* **2001**, *212* (1), 11-34.
(10) Burton, V. J.; Deeth, R. J.; Kemp, C. M.; Gilbert, P. J. Molecular mechanics for coordination complexes: the impact of adding d-electron stabilization energies. *Journal of the American Chemical Society* **1995**, *117* (32), 8407-8415.
(11) Deeth, R. J.; Foulis, D. L. Analytical derivatives, π bonding and d–s mixing in the ligand field molecular mechanics method. *Physical Chemistry Chemical Physics* **2002**, *4* (18), 4292-4297.
(12) Lemkul, J. A.; Huang, J.; Roux, B.; MacKerell, A. D., Jr. An Empirical Polarizable Force Field Based on the Classical Drude Oscillator Model: Development History and Recent Applications. *Chemical Reviews* **2016**, *116* (9), 4983-5013. DOI: 10.1021/acs.chemrev.5b00505.
(13) Lamoureux, G.; Roux, B. t. Modeling induced polarization with classical Drude oscillators: Theory and molecular dynamics simulation algorithm. *The Journal of Chemical Physics* **2003**, *119* (6), 3025-3039. DOI: 10.1063/1.1589749 (acccessed 3/21/2024).
(14) Lamoureux, G.; Harder, E.; Vorobyov, I. V.; Roux, B.; MacKerell, A. D. A polarizable model of water for molecular dynamics simulations of biomolecules. *Chemical Physics Letters* **2006**, *418* (1), 245-249. DOI: https://doi.org/10.1016/j.cplett.2005.10.135.
(15) Dajnowicz, S.; Ghoreishi, D.; Modugula, K.; Damm, W.; Harder, E. D.; Abel, R.; Wang, L.; Yu, H. S. Advancing free-energy calculations of metalloenzymes in drug discovery via implementation of LFMM potentials. *Journal of Chemical Theory and Computation* **2020**, *16* (11), 6926-6937.
(16) Jensen, F. Unifying Charge-Flow Polarization Models. *Journal of Chemical Theory and Computation* **2023**, *19* (13), 4047-4073.
(17) Rappe, A. K.; Goddard, W. A., III. Charge equilibration for molecular dynamics simulations. *The Journal of Physical Chemistry* **1991**, *95* (8), 3358-3363. DOI: 10.1021/j100161a070.
(18) Chen, J.; Martínez, T. J. QTPIE: Charge transfer with polarization current equalization. A fluctuating charge model with correct asymptotics. *Chemical physics letters* **2007**, *438* (4-6), 315-320.
(19) Dougherty, D. A. Cation-pi interactions in chemistry and biology: a new view of benzene, Phe, Tyr, and Trp. *Science* **1996**, *271* (5246), 163-168. DOI: 10.1126/science.271.5246.163 From NLM Medline.
(20) Ponder, J. W.; Case, D. A. Force fields for protein simulations. *Advances in protein chemistry* **2003**, *66*, 27-85.
(21) Brooks, B. R.; Bruccoleri, R. E.; Olafson, B. D.; States, D. J.; Swaminathan, S. a.; Karplus, M. CHARMM: a program for macromolecular energy, minimization, and dynamics calculations. *Journal of computational chemistry* **1983**, *4* (2), 187-217.

(22) Kumar, K.; Woo, S. M.; Siu, T.; Cortopassi, W. A.; Duarte, F.; Paton, R. S. Cation–π interactions in protein–ligand binding: theory and data-mining reveal different roles for lysine and arginine. *Chemical Science* **2018**, *9* (10), 2655-2665, 10.1039/C7SC04905F. DOI: 10.1039/C7SC04905F.
(23) Maple, J. R.; Cao, Y.; Damm, W.; Halgren, T. A.; Kaminski, G. A.; Zhang, L. Y.; Friesner, R. A. A Polarizable Force Field and Continuum Solvation Methodology for Modeling of Protein−Ligand Interactions. *Journal of Chemical Theory and Computation* **2005**, *1* (4), 694-715. DOI: 10.1021/ct049855i.
(24) Springs, B.; Haake, P. Equilibrium constants for association of guanidinium and ammonium ions with oxy anions the effect of changing basicity of the oxy anion. *Bioorganic Chemistry* **1977**, *6* (2), 181-190.
(25) Groom, C. R.; Bruno, I. J.; Lightfoot, M. P.; Ward, S. C. The Cambridge structural database. *Acta Crystallographica Section B: Structural Science, Crystal Engineering and Materials* **2016**, *72* (2), 171-179.
(26) Wang, R.; Fang, X.; Lu, Y.; Wang, S. The PDBbind database: Collection of binding affinities for protein− ligand complexes with known three-dimensional structures. *Journal of medicinal chemistry* **2004**, *47* (12), 2977-2980.
(27) Hay, P. J.; Wadt, W. R. Ab initio effective core potentials for molecular calculations. Potentials for the transition metal atoms Sc to Hg. *The Journal of chemical physics* **1985**, *82* (1), 270-283.
(28) Lin, Y.-S.; Li, G.-D.; Mao, S.-P.; Chai, J.-D. Long-range corrected hybrid density functionals with improved dispersion corrections. *Journal of Chemical Theory and Computation* **2013**, *9* (1), 263-272.
(29) Weigend, F. Accurate Coulomb-fitting basis sets for H to Rn. *Physical chemistry chemical physics* **2006**, *8* (9), 1057-1065.
(30) Wang, L.; Wu, Y.; Deng, Y.; Kim, B.; Pierce, L.; Krilov, G.; Lupyan, D.; Robinson, S.; Dahlgren, M. K.; Greenwood, J.; et al. Accurate and Reliable Prediction of Relative Ligand Binding Potency in Prospective Drug Discovery by Way of a Modern Free-Energy Calculation Protocol and Force Field. *Journal of the American Chemical Society* **2015**, *137* (7), 2695-2703. DOI: 10.1021/ja512751q.
(31) Salonen, L. M.; Bucher, C.; Banner, D. W.; Haap, W.; Mary, J.-L.; Benz, J.; Kuster, O.; Seiler, P.; Schweizer, W. B.; Diederich, F. Cation–π Interactions at the Active Site of Factor Xa: Dramatic Enhancement upon Stepwise N-Alkylation of Ammonium Ions. *Angewandte Chemie International Edition* **2009**, *48* (4), 811-814. DOI: https://doi.org/10.1002/anie.200804695 (acccessed 2024/03/21).
(32) Schmidt, T. C.; Eriksson, P.-O.; Gustafsson, D.; Cosgrove, D.; Frølund, B.; Boström, J. Discovery and Evaluation of Anti-Fibrinolytic Plasmin Inhibitors Derived from 5-(4-Piperidyl)isoxazol-3-ol (4-PIOL). *Journal of Chemical Information and Modeling* **2017**, *57* (7), 1703-1714. DOI: 10.1021/acs.jcim.7b00255.
(33) Oganesyan, V.; Damschroder, M. M.; Cook, K. E.; Li, Q.; Gao, C.; Wu, H.; Dall'Acqua, W. F. Structural Insights into Neonatal Fc Receptor-based Recycling Mechanisms. *Journal of Biological Chemistry* **2014**, *289* (11), 7812-7824. DOI: 10.1074/jbc.M113.537563 (acccessed 2024/03/21).
(34) Acqua, W. F. D.; Woods, R. M.; Ward, E. S.; Palaszynski, S. R.; Patel, N. K.; Brewah, Y. A.; Wu, H.; Kiener, P. A.; Langermann, S. Increasing the affinity of a human IgG1 for the

neonatal Fc receptor: biological consequences. *The Journal of Immunology* **2002**, *169* (9), 5171-5180.